Supporting Information

Defect-Tolerant TiO_2-Coated and Discretized Photoanodes for >600 h of Stable Photoelectrochemical Water Oxidation

Xin Shen[ab], Maoqing Yao[c], Ke Sun[d], Tianshuo Zhao[ab], Yulian He[ab], Chun-Yung Chi[c], Chongwu Zhou[c], Paul Daniel Dapkus[c], Nathan S. Lewis*[d] and Shu Hu*[ab]

Author Affiliations:

[a] Department of Chemical and Environmental Engineering, School of Engineering and Applied Science, Yale University, New Haven, Connecticut 06520, United States.

[b] Energy Sciences Institute, Yale West Campus, West Haven, Connecticut 06516, United States.

[c] Department of Electrical Engineering, University of Southern California, Los Angeles, California 90089, United States.

[d] Division of Chemistry and Chemical Engineering, California Institute of Technology, Pasadena, California 91125, United States.

*Corresponding authors: shu.hu@yale.edu, nslewis@caltech.edu

This PDF file includes:

S1 Methods

1.1 Chemicals and Materials

Bis(cyclopentadienyl)iron (II) (ferrocene, $Fe(Cp)_2$) and bis(cyclopentadienyl)cobalt(II) were purified by sublimation of the as-received chemicals from Sigma Aldrich. Bis (cyclopentadienyl)iron(III)tetrafluoroborate and bis(cyclopentadienyl)cobalt(III) hexafluoro-phosphate were both recrystallized in a mixture of diethyl ether (ACS grade, EMD) and acetonitrile (ACS grade, EMD), and dried in vacuo before use. $K_3Fe(CN)_6$ (Fisher Scientific, 99.4%), $K_4Fe(CN)_6$ (Fisher Scientific, 99.4%), and KOH (Fisher Scientific, >85%) were used as received.

Both Si and GaAs wafers were used as substrates for growth of GaAs nanowires, with wafer specifications as follows: n-Si ((111)-oriented, Phosphorus-doped with a resistivity $\rho = 1 – 10$ Ω·cm, 4" diameter, Addison Engineering, Inc.); n^+-Si ((111)-oriented, As-doped with $\rho < 0.002$ Ω·cm, 4" diameter, Addison Engineering, Inc.); n^+-GaAs ((111)B-oriented, Si-doped with $\rho < 0.005$ Ω·cm, 2'' diameter, AXT Inc.); and p^+-GaAs ((111)B-oriented, Zn-doped with $\rho < 0.002$ Ω·cm, 2'' diameter, AXT Inc.). 18.2 MΩ·cm resistivity deionized H_2O was obtained from a Millipore system.

1.2 Planar np^+-Si (111) as Growth Substrates

An np^+-Si buried junction was formed by boron-ion implantation (45 keV energy with a dose of 1×10^{14} cm^{-2} first and then 32 keV energy with a dose of 5×10^{14} cm^{-2}) onto the front side of a (111)-oriented n-Si wafer. A back-surface field was formed by phosphorus-ion implantation onto the backside of the n-Si wafer (140 keV energy with a dose of 1×10^{14} cm^{-2} first and then 75 keV energy with a dose of 5×10^{14} cm^{-2}), followed by a rapid thermal anneal at 1000 ºC for 15 s in an N_2(g) atmosphere to induce solid-phase regrowth on both sides and to activate the dopants.

Secondary-ion mass spectrometry measurements showed an averaged doping concentration of 1×10^{19} cm^{-3} for the top 75-nm layer on the front side of the Si. The np^+-Si buried junctions exhibited an open-circuit photovoltage of ~ 0.55 V under simulated 1-sun illumination.

1.3 MOCVD Growth of GaAs Nanowires

Single-crystalline, (111)B-oriented, n^+-GaAs wafers were used as epitaxial growth substrates for GaAs nanowires. An array of n-GaAs nanowire cores was grown in a single temperature step of 760 ºC for 30 min, in the gas mixture of trimethylgallium (TMGa) at 7.51×10^{-7} atm, arsine (As_2H_6) at 2.13×10^{-4} atm, and diluted disilane (Si_2H_6, 500 ppm in H_2) at 1.42×10^{-8} atm as an n-type dopant source. Hydrogen was the carrier gas. The n-type doping of GaAs nanowires under this Si_2H_6 partial pressure was calibrated to be $2.5 – 3.0 \times 10^{18}$ cm^{-3}, according to a previous publication.[1] The partial pressure of the Ga and As precursors and the dopant gas concentrations were chosen to achieve optimal photoactivity for the as-grown GaAs nanowires, and their energy-conversion properties were confirmed following published procedures.[1]

GaAs nanowires of the same optimal photoactivity were then grown on a Si (111) substrate that was a planar np^+-junction absorber. Before growth, the electron-beam patterned SiN_x mask, which was created on the Si growth substrate following the same fabrication process as reported in a previous study.[1-2] SiN_x mask is 50-nm thick, deposited by plasmonic enhanced chemical vapor deposition. Electron beam lithography (Vistec EBPG 5000+) was followed by reactive ion etching (CHF_3, 50 Torr, 100 W). The process created an array of well-defined holes in the SiN_x mask. Then the sample was etched for 30 s with 1.0 M hydrofluoric acid (HF), and the substrate was then immediately loaded into the MOCVD reactor. The substrate was annealed for 5 min at 920 ºC in H_2(g) to remove residual native silicon oxides in the nanoscale openings of the SiN_x mask. The temperature was lowered to 440 ºC in an As_2H_6 atmosphere to form a preferred surface

reconstruction for the growth of GaAs nanowires. The identical selective-area growth condition was used to grow GaAs nanowires on (111) B-oriented GaAs substrates.

An ohmic contact that was formed during growth consisted of a degenerately doped n^+-GaAs seed layer (5 – 10 nm) and a degenerately doped p^+-Si top surface (~ 75 nm) between the GaAs top and the Si bottom absorbers.[3] The dopant concentration for the n^+-GaAs seed layer was set at 4×10^{18} cm^{-3} according to calibration runs. The p^+-Si top layer had p-type doping at a level of 1×10^{19} cm^{-3}. Device modeling indicated ohmic behavior of n^+-GaAs/p^+-Si interfaces at the milliampere level (see Section 2.1 **"**Simulation of p^+-Si/n^+-GaAs Junctions"). Furthermore, similar Si/InAs heterojunctions having comparable levels of degenerately n^+- and p^+-type doping exhibit trap-assisted tunneling that results in low contact resistance.[4-5] We have consequently used the n^+-GaAs/p^+-Si combination as a low-resistance ohmic contact, as this combination allows for direct integration of proper ohmic contacts or tunnel junctions into the nanowire-on-Si fabrication process.

1.4 Surface Chemistry of As-Grown GaAs Nanowires

Prior to ALD growth of TiO_2 protection layers, GaAs nanowires were etched for 30 s in a solution of Br_2 (0.04% v/v, Acros Organics) in CH_3OH (low water, J.T. Baker), followed by a rinse with H_2O and immersion for 15 s in 1.0 M KOH(aq). The bare GaAs nanowires on the sample were rinsed with H_2O, dried in a stream of N_2(g), and quickly transferred to an ALD chamber for growth of amorphous TiO_2 (*a*-TiO_2). The GaAs nanowire photoelectrode underwent the same surface treatment before measurements in a non-aqueous photoelectrochemical cell. For non-aqueous photoelectrochemistry, the bare GaAs nanowires on a photoelectrode were etched and then immediately loaded via an anti-chamber into an N_2(g)-purged glovebox.

1.5 Atomic Layer Deposition of Amorphous TiO_2

The *a*-TiO_2 coating was deposited on the GaAs nanowire tops and sidewall surfaces at 150 °C using a Cambridge Nanotech Savannah S200 atomic-layer deposition (ALD) system or a Fiji G2 system, but with no difference in the film property. Each ALD cycle consisted of a 0.015 s pulse of N_2-purged H_2O, followed by a 0.10 s pulse of tetrakis-dimethylamido titanium (TDMAT, Sigm*a*-Aldrich, 99.999%, used as received). A 15 s purge under a constant flow of high-purity N_2(g) was performed between each precursor pulse. TiO_2 coatings with thicknesses of ~ 100 nm were conformally deposited onto the nanowire-array samples, according to a planar growth rate of 0.047 nm per cycle. The coating thickness was confirmed by SEM (**Figures 2b and 2c**) and TEM (**Figure 2d**) measurements.

1.6 Deposition of NiO_x Electrocatalyst

NiO_x was deposited by reactive RF magnetron sputtering (AJA International) on both *a*-TiO_2-protected GaAs planar samples and GaAs nanowire array samples. Sputtering was performed with a metallic Ni target at 150 W and at a pressure of 5 mTorr, under a continuous flow of 20 sccm Ar(g) and 0.5 sccm of O_2(g). This condition was optimized for conformal deposition. The substrate was not intentionally heated, and the deposition time was 10 min, which resulted in a planar equivalent thickness of ~ 10 nm. The as-fabricated planar Si/NW GaAs/*a*-TiO_2/NiO_x structure is shown schematically in **Figure S2.**

1.7 Photoelectrochemical (PEC) Measurements

The intrinsic energy-conversion properties of the planar Si/NW GaAs/*a*-TiO_2/NiO_x photoanodes were characterized using non-aqueous PEC experiments. A dry acetonitrile (CH_3CN, anhydrous, 99.8%, Sigma Aldrich) solution of 1.0 M $LiClO_4$ (dried by fusing the battery-grade

salt in vacuo) containing the appropriate redox species was used to contact the photoanodes. Electrochemistry was performed in a three-electrode PEC cell in an N_2(g)-purged glovebox. The reference electrode was a Pt wire (0.5 mm diameter, 99.99% trace metals basis, Alfa-Aesar), and the counter electrode was a Pt gauze (100 mesh, 99.9% trace metal basis, Alfa-Aesar). Table S2 lists the PEC cell configuration used in this study. The redox systems were listed in Table S3: a ferrocenium (5 mM)/ferrocene (50 mM) solution, a decamethylferrocenium (5 mM)/ decamethylferrocene (50 mM) solution, and a cobaltocenium (10 mM)/cobaltocene (50 mM) solution. The Xe lamp used is Newport model #6254. The AM 1.5 G filter refers to the #81094 Air Mass Filter (Newport), which corrects the output of a xenon lamp to better match the total (direct and diffuse) spectrum when the sun is at a zenith angle of 37.0°. As illustrate in Fig. S3c, prior to PEC experiments, a light intensity calibration was conducted where two Si photodiodes are used. The Si photodiode #1 was placed at the exact position of the working electrode, while the photodiode #2 was placed in air (outside of the cell), but also fixed at the location, facing to the light source. From the calibration, the light intensity reach to photodiode #1 was adjusted and fixed to be one-sun, while the photodiode #2 is used as the reference to show the time-dependence of the light intensity.

Aqueous PEC experiments were used to evaluate the current density vs potential behavior, spectral response, stability, and Faradaic efficiency of the *a*-TiO_2-coated photoelectrodes. In this three-electrode configuration depicted in **Figure S3a**, a Pt wire (0.5 mm diameter, 99.99% trace metals basis, Alf*a*-Aesar) was used as a reference electrode, and a Pt gauze was used as the counter electrode (summarized in **Table S1b**). The one-electron aqueous redox couple, $Fe(CN)_6^{3-/4-}$ (50 mM $K_3Fe(CN)_6$ and 350 mM $K_4Fe(CN)_6$), was used to assess the energy-conversion properties of

a-TiO_2-coated GaAs nanowire photoanodes without complications arising from interfacial kinetics of water oxidation.

When NiO_x electrocatalysts were deposited on planar or nanowire-array samples, the *a*-TiO_2-coated photoanodes were evaluated for water oxidation in 1.0 M KOH(aq). The reference electrode was mercury/mercury oxide (Hg/HgO, 1.0 M KOH filling solution, CH Instruments), and the counter electrode was a carbon rod in a fritted glass tube. The formal potential for the oxidation of OH^- (aq) to O_2(g), i.e., 0.33 V vs. Hg/HgO, was calculated from the measured pH of the solution (pH=13.6) in conjunction with the value provided by CH Instruments, which is E(Hg/HgO) = 0.098 V vs. NHE at 25 °C. Consistently, the open-circuit potential of a NiO_x film electrode in the KOH(aq) electrolyte was measured to be 0.33 V vs. Hg/HgO.

Simulated Air Mass (AM) 1.5G illumination, as well as ELH-type bulb and ENH-type bulb tungsten-halogen lamp illumination, were used for photoelectrochemical experiments. AM 1.5 simulated illumination was obtained by the use of a Xe lamp with an AM 1.5G filter. The illumination intensity was calibrated by placing a Si photodiode (FDS100, Thor Labs) in the electrolyte-containing electrochemical cell in the same location as the photoelectrode during PEC measurements. For light-dependent measurements, the light intensity was attenuated with a series of neutral-density filters. All PEC measurements were performed using a Biologic SP-200 potentiostat. All electrode areas were reported as geometric areas, as determined by a calibrated optical scanner that digitally recorded the electrode dimensions.

We have examined this electrode under dark conditions over a short period. During the 600-hour stability test, the light was turned off for twice, each time for 20 minutes, but we did not observe corrosion or current decay from the repeated experiment (Figure S14). Typically, the illumination to photoanodes aggravates corrosion significantly, while in the dark, the chemical

corrosion takes place just as it occurs under illumination. We confirm that the dark corrosion does not occur or has a very slow corrosion rate. Therefore, our testing condition has relevance to diurnal or intermittent field operation conditions, provided that the light intensity, surface potentials, and cumulative charges are comparable. The stability result of the electrode under our photo-corrosion conditions represents a rigorous photoanodic testing condition, and supported our photo-corrosion mitigation strategy. We therefore note that the dark corrosion of equal duration for the nanoscale Si opening needs to be further investigated.

1.8 Spectral Response of Tandem Si/GaAs Photoanodes

The spectral response, or external quantum yield, Φ_{ext}, measures the quantum efficiency as a function of wavelength. Monochromatic light (at a 10-nm bandwidth and chopped at 27 Hz) was generated using a computer-controlled monochromator (Newport Corp.). The monochromatic light was focused to a spot size that under-filled the active area of the tandem photoelectrode, so the effect of light scattering from the photoelectrode edge is negligible. The spectral response of the top GaAs nanowire junction was measured by passing the output of a fiber lamp that provided continuous illumination through a long-pass filter (cut-off wavelength of 950 nm), thereby saturating the Si bottom junction. Conversely, the spectral response of the Si bottom junction was measured while the GaAs top junction was saturated by a light-emitting diode (LED) with a 405-nm fundamental emission wavelength. When the spectral response of the Si bottom cell was measured, the light was filtered by the GaAs nanowire top cell. Measurements were performed at several potentials (e.g., 1.5 – 1.9 V vs RHE) to ensure full extraction of photogenerated carriers in the tandem photoanode. Calibration of the irradiance provided by the monochromatic light was performed using a bottom-facing Si calibration photodiode (FDS100-CAL, Thor Labs) that was placed in the electrolyte-containing electrochemical cell at the same location as the photoelectrode.

These spectral response data were collected under potentiostatic control at 1.9 V vs RHE (1.0 V vs Hg/HgO) for the top GaAs absorber and at 1.5 V vs RHE (0.6 V vs Hg/HgO) for the bottom Si absorber, respectively.

1.9 Faradaic Efficiency for Water Oxidation

The Faradaic efficiency for oxygen evolution of a tandem planar Si/nanowire array GaAs /*a*-TiO_2-coating/NiO_x-catalyst photoanode was measured in the same electrochemical setup as used for the *J-E* and spectral response measurements. The potential was set to operate at a light-limited photocurrent density under 1-sun illumination. The solution (~ 55 mL in volume) was purged with N_2(g) for > 2 h to obtain a nearly oxygen-free environment. Then, after a 10-min waiting period at open circuit, the nanowire array photoanode was held at 1.50 V vs RHE (0.6 V vs Hg/HgO) for 30 min.

The O_2(g) concentration in the solution was measured over the entire 30 min period with an Ocean Optics fluorescent probe (NeoFox HIOXY). The amount of charge passed (*Q*) vs. time (min) was plotted assuming 100% Faradaic efficiency, i.e., assuming that 4 electrons were used to generate 1 oxygen molecule, or equivalently that 0.33 mA h of charge passed generated 100 μg of O_2(g). The data that represented the oxygen concentration vs time were then converted to micrograms of O_2 vs time. The resultant data were plotted together with the *Q* vs *t* data, using the amount of O_2 dissolved in water at room temperature under 1 atm (7700 μg L^{-1}), the solution was stirred continuously to avoid trapping bubbles on the nanowire array electrode and to minimize undesirable spikes in the dissolved oxygen concentration. The illumination was turned off after 30 min.

S2 Supplementary Discussions

S2.1 Simulation of p^+-Si/n^+-GaAs Junctions

To support the presence of an ohmic contact between the n^+-GaAs and p^+-Si layers, a 1-D device model in SCAPS (University of Gent, Belgium) was built to simulate the multilayer solid-state junction between the np^+-Si planar bottom cell and an n-GaAs nanowire, with and without the n^+-GaAs seed layer, respectively. As shown in **Figure S2**, after inserting a 10 nm-n^+-GaAs layer, the band bending in GaAs became steeper at the junction interface, at which electrons and holes recombine. The steep band bending facilitated tunneling of electrons from the GaAs and tunneling of holes from the Si. As a result, the simulation showed a reduced contact resistance, i.e., 1/43 of the original value, due to the introduction of the n^+-GaAs seed layer. As a result of MOCVD growth of an n^+-GaAs seed layer on p^+-Si, this junction design can improve the ohmic conductivity between the two tandem junctions, allowing more than 10 mA cm^{-2} of photocurrent density to pass.

S2.2 Photoelectrochemical Behavior of Tandem Planar Si/Nanowire GaAs Photoanodes

The photoanode behavior at 1-sun and ~1.7-sun intensity are shown in **Figure 3b** and in **Figure S5 (**red curve), respectively. Both light intensities gave comparable photoanodic onset potentials of 0.92 V vs RHE in 1.0 M KOH(aq). The onset potentials for water oxidation in the dark were evaluated using a planar p^+-GaAs /nanowire array p^+-GaAs /*a*-TiO_2/NiO_x dark anode grown on a p^+-GaAs (111)B planar substrate (black curve), or by extracting the dark current onset of the planar Si/nanowire GaAs photoanode measured in the dark (green curve). Both methods gave a photocurrent onset potential of ~ 1.65 V vs RHE. By calculating the shift of the water-oxidation onset potentials under illumination as compared with the dark, the planar Si/nanowire array GaAs photoanode produced a potential shift of – 0.72 ± 0.07 V. This potential shift is slightly

different from the measured open-circuit photovoltage, possibly due to inaccuracies arising from the use of onset potentials to estimate photovoltages.

A comparison of the currents measured both in the dark (green curve) and under illumination (red curve) indicated a leakage current, as shown in **Figure S5**. The leakage pathway is indicative of anodic charge injection from Si back contacts to the electrolyte. This leakage current was possibly due to the hole transport from the np^+-Si junction and the degenerately doped n^+-GaAs seed layer at the planar Si/ nanowire GaAs interface, directly through *a*-TiO_2 coatings, and then to the NiO_x electrocatalysts. This leakage current bypassed the conduction through the GaAs-nanowire absorber. Both nanowire p^+-GaAs/*a*-TiO_2/NiO_x anodes and nanowire n-GaAs/*a*-TiO_2/NiO_x photoanodes grown on planar GaAs showed a positive corrosion current, as observed in a potential range of 0.9 – 1.7 vs RHE, but such an anodic corrosion current was not observed for the GaAs-nanowire-on-Si photoanodes.

S2.3 Energy-Conversion Properties of Top GaAs and Bottom Si Absorbers

The PEC energy-conversion properties of the top GaAs nanowire and the bottom Si planar junctions were studied separately: each light absorber was made into photoelectrodes, and their respective energy-conversion properties were evaluated. The energy-conversion properties of *a*-TiO_2-coated GaAs nanowire array single-absorber photoelectrodes were evaluated in contact with both aqueous $Fe(CN)_6^{3-/4-}$ and non-aqueous $Fe(Cp)_2^{+/0}$ electrolytes. The planar np^+-Si (see **Table S1**) bottom absorber was tested in a non-aqueous $Fe(Cp)_2^{+/0}$ electrolyte for evaluation of its energy-conversion performance. The planar np^+-Si photoelectrode showed an open-circuit photovoltage of 0.53 V and a photocurrent density of ~ 35 mA cm^{-2} under 1-sun illumination in contact with the non-aqueous $Fe(Cp)_2^{+/0}$ redox system **(Figure S8)**, in accordance with the prior reports of the behavior of np^+-Si buried-junction cells.[6-7]

Figure S6a shows the light-dependent *J-E* behavior of n-type GaAs nanowires grown on an n^+-doped planar GaAs (GaAs planar/ GaAs NW) photoelectrode in contact with the CH_3CN-$Fe(Cp)_2^{+/0}$ redox system (0.5 mM $Fe(Cp)_2^+$– 90 mM $Fe(Cp)_2$) in non-aqueous electrolytes, under a range of illumination intensities between 0.25 – 1 sun. The as-grown GaAs nanowire arrays produced J_{ph} = 12.2 mA cm^{-2} at 1 Sun and exhibited an open-circuit potential of −0.64 V vs the Nernstian potential of the non-aqueous electrolyte ($E(Fe(Cp)_2^{+/0})$). A diode-quality factor of 2.5 was obtained from the *J*–*E* data as a function of illumination intensity.[1, 7] The photovoltages of as-grown GaAs nanowire arrays in contact with different redox couples in non-aqueous electrolytes are shown in **Table S3**. These redox couples span a 1.3 V difference in electrochemical potentials, and yet the photovoltages measured for the nanowire arrays varied over a range of 350 mV, indicating a contact-dependent performance of GaAs nanowire/liquid junctions.

Figure S6b shows the *J-E* behavior of the planar GaAs /NW GaAs /*a*-TiO_2/NiO_x photoanode (**see from Table S1**) in contact with the aqueous 50 mM $Fe(CN)_6^{3-}$/ 350 mM $Fe(CN)_6^{4-}$ redox system, under ENH-type tungsten-halogen illumination at 1-sun (red curve). This TiO_2-coated photoelectrode exhibited a light-limited photocurrent density of J_{ph} = 5.11 mA cm^{-2}, a photovoltage of E_{oc} = − 0.22 V vs. $E(Fe(CN)_6^{3-/4-})$, and a fill factor, i.e. *ff* = 0.20.

S2.4 Discussion of Quantum Yields and Faradic Efficiency

The external quantum yields (Φ_{ext}) and Faradaic efficiency were further quantified for the planar Si /NW GaAs /*a*-TiO_2/NiO_x photoanode. **Figure S7a** shows Φ_{ext} vs wavelength measured in 1.0 M KOH (aq). The spectral response of the top GaAs nanowire absorber was mostly independent of applied potential for E > 1.50 V vs RHE. For the bottom Si absorber, Φ_{ext} increased over the full wavelength range when the applied anodic potential increased above E > 1.50 V vs RHE, until Φ_{ext} became light-limited at 1.90 V vs RHE. This potential ensured the full extraction of

photogenerated carriers because the tandem photoanode exhibited a light-limited current density in this potential range (**Figure S6**). The *J-E* behavior further corroborates the spectral response behavior, because the integration of the Φ_{ext} values of the top GaAs and bottom Si cells with respect to the AM 1.5G spectrum produced calculated light-limited current densities of 9.3 mA cm^{-2} and 8.3 mA cm^{-2}, respectively. These calculated photocurrent densities are consistent with the light-limited photocurrent density (J_{ph}) of 9.1 ± 0.9 mA cm^{-2} measured at 1 sun. Further optimization for the current matching between GaAs nanowire top and Si bottom absorbers can be achieved via control of the geometry and morphology of the wire arrays.[8] Specifically, patterns of SiN_x mask openings can define the size, pitch, and shape of the GaAs nanostructures, and the nanowire height can be determined by the growth time.

The quantitative oxygen evolution of the Si planar /GaAs NW /*a*-TiO_2/NiO_x photoanode is shown in **Figure S7b**. A comparison between the amount of charge passed and the amount of O_2(g) dissolved in water indicated ~ 100% Faradaic efficiency for O_2(g) production, as expected based on the reported ~ 100% Faradaic efficiency of protected planar GaAs photoanodes. [6]

S2.5 Comparison Among Planar Si/ NW GaAs/*a*-TiO_2/NiO_x, Planar GaAs/*a*-TiO_2/NiO_x, and Planar GaAs /NW GaAs/*a*-TiO_2/NiO_x Photoelectrodes

To confirm the defect-tolerant behavior of planar Si/NW GaAs/*a*-TiO_2/NiO_x photoanodes towards photocorrosion, stability tests, and SEM morphology characterizations were also conducted by using planar n-GaAs/*a*-TiO_2/NiO_x and planar GaAs/NW GaAs/*a*-TiO_2/NiO_x structures as a control. The thickness of the *a*-TiO_2 protective coating and the Ni/NiO_x catalysts were kept at the same values of ~ 100 nm and ~ 10 nm, respectively, for evaluating their long-term stability and defect tolerance.

In contrast to the >600 h stability of planar Si /NW GaAs /*a*-TiO_2/NiO_x, a series of visible corrosion pits developed on the planar n-GaAs/*a*-TiO_2/NiO_x photoanode surface after 10 h of continuous operation under illumination (**Figure S9**). For the defect regions, the TiO_2 coating was either lifted off. or stay free-standing above the undercut GaAs substrate, as reported in recent work by Yu et. al.[9] This morphology was consistent with a pitting corrosion mechanism in which defects in the coating initiated the pitting corrosion of the photocorrosion susceptible substrate, such as GaAs. These corrosion pits then readily propagated to nearby regions (depicted in **Figure 1a**). The observed behavior was consistent with a full characterization of the size distribution and origin of the defects, as well as the short-term and long-term failure mechanisms for *a*-TiO_2-coated GaAs. The failure process was even more rapid and catastrophic for the planar GaAs /NW GaAs /*a*-TiO_2/NiO_x photoanode as the control than for the planar GaAs photoanode. During a 30-minute stability test, the entire GaAs nanowire array lifted-off, along with the *a*-TiO_2 coatings and NiO_x catalysts (**Figure S10**), leaving a large hole on the electrode surface and exposing the etched GaAs substrate. Therefore, fabrication of corrosion-susceptible light absorbers such as III-V semiconductors into nanostructures, despite its advantage in light trapping, does not produce prolonged stability necessarily. The key to obtaining corrosion resistance is the use of self-passivating substrate materials to support discrete, corrosion-susceptible light absorbers, as described in the main text.

S2.6 Extended Discussion of the Corrosion Behavior of Planar Si /NW GaAs/*a*-TiO_2/NiO_x Photoanodes

The water-oxidation stability data (**Figure 3**), and SEM and EDS characterizations (**Figure 4**) presented in the main text collectively support the claim that tandem Si planar /NW GaAs /*a*-TiO_2/NiO_x photoanodes exhibit extended stability. Changes in the nanowire structure and

composition were further investigated: after the 600-h stability test, the photoanode was sonicated to shake off a few TiO_2-coated nanowires that remained on the electrode surface. TEM images and EDS mapping for one of the representative nanowires are presented in **Figure S11**. The data indicate that the sonicated nanowires maintained their structural and compositional integrity after the 600-h stability test. Nevertheless, the current did experience a ~10% decay after a 600-hour test. A recent study about failure modes of *a*-TiO_2 coated GaAs photoanode reported that there could be two corrosion mechanism contributing to this decay during the 600-hours operation. One is associated with the short-term stability (from extrinsic defects such as external particulate matters), while the other is related to the long-term stability (usually from intrinsic defects that arise during operation).[10] In our case, there was no apparent current decay at the beginning stage of the test. We postulate there could be two explanations: 1) The density of extrinsic defects was low. Therefore the current drop was not prominent; and 2) The decay happened during the CV scan before the start of the stability test. The ~10% decay was mainly due to the corrosion mechanism associated with the emergence of the pinhole defects. The signal loss of Ti (Figure 4n) is one evidence to this transformation. More detailed discussions about why and how this transformation happen can be referred to the recent study by Ros et al.[11] But one differentiation point is that our *a*-TiO_2 is different from the polycrystalline TiO_2 with grain boundaries that this study used. So, to ascertain the real failure mode of long-term stability of this specific design, further follow-up study is needed. Since we have not run the test for longer duration, we are cautious not to simply extrapolating the decay rate over longer period.

Density counts for the nanowires before and after the test (Table S2) showed that, on average, the electrode surface lost ~ 5% of the nanowires, whereas the photocurrent density decreased by ~ 9%. Two additional planar Si /NW GaAs /*a*-TiO_2/NiO_x photoanodes that used

thinner *a*-TiO_2 coatings, i.e., 20 nm and 5 nm, respectively, were also fabricated. These samples were tested under identical operational conditions as described above, with SEM monitoring changes in surface morphology after water oxidation (**Figures S12 and S13**). A more substantial fraction of nanowires peeled off from the photoanode that was coated with 20-nm *a*-TiO_2 as compared to the 100-nm *a*-TiO_2 coated tandem planar Si /NW GaAs photoanode. The sites where nanowires peeled off appeared randomly in the array. **Figure S13** further shows that for samples with a 5-nm *a*-TiO_2 coating, the loss of nanowires occurred within 50 h of operation, and defective regions on the electrode surface spread to the neighboring regions. After the testing, in some cases, the defects or imperfections inside the thin TiO_2 coating might not be discrete but somewhat connected; or in other cases, during photocorrosion, the thin coating might become semi-permeable to soluble reactants, such as hydroxide (OH^-) ions, and soluble products, such as gallium (Ga^{3+}) ions. In these cases, the thin coating could not effectively isolate or contain the corrosion defects. When the coating was too thin (<20 nm), more defects exist in the coating so that underlying SiN_x masks and Si layers are exposed and become susceptible to corrosion and dissolution. Too thin coatings fail to limit the dissolution of the underlying SiN_x and Si layers, and fail to contain the corrosion front to propagate readily (see **Figure S13a**). These observations are consistent with the hypothesis that the initial failure mechanism of the protected tandem photoanode originates from imperfections in the *a*-TiO_2 coating. These defects or imperfections that are created during ALD growth or water oxidation allow small and soluble ions, such as hydroxide ions, to permeate through the coating and initiate the corrosion of the GaAs nanowire cores. When the *a*-TiO_2 coating is thick enough, e.g., 100-nm thick, the failure point is relatively random and sporadic. In this case, a defect on *a*-TiO_2 coatings should only affect individual nanowires. When the coating is thinner than 20 nm, the percentage of nanowires that have defects

in their coating shells increases substantially, causing more nanowires to peel off in less than 50 h. Therefore, thin coatings preclude the extended photoelectrode operation due to insufficient protection of individual isolated nanowires.

Another observation was that the corrosion of this 5-nm TiO_2 electrode appeared to start from the marginal regions. This behavior may result from an uneven light intensity distribution, or the galvanic effect. On the edge of the array, the GaAs nanowires may exhibit different potentials and uneven charge distribution, as compared with the area covered by SiN_x masks. But more evidence is needed for ascertaining this factor, which is beyond the discussion of this work.

Regarding the correlation between the *a*-TiO_2 thickness and defect density, one recent work mention the pinhole density decreased substantially when the thickness of the *a*-TiO_2 coating increased beyond 45 nm, and approached zero when the thickness of the film exceeded 112 nm.[10] This work also pointed out the emergent pinholes that occurs during the test were unavoidable for a range of coating thicknesses. To conclude from the above discussion, when coating thickness is <100 nm, thicker *a*-TiO_2 can significantly enhance the electrode stability. In this thickness range, the *a*-TiO_2 can be considered as highly conductive layer. Considering the trade-off between the performance and stability, the optimal thickness of *a*-TiO_2 is recommended to be around 100 nm. However, when the coating is thicker than 143 nm, the resistance starts to build up therefore it is less desirable.[6]

S2.7 The reproducibility of the high stability of the Planar Si /NW GaAs/*a*-TiO_2/NiO_x Photoanodes

To examine the reproducibility of the high stability we observed from the 600-hour test, three photoanodes of the same structure and composition were tested, and all showed comparable stability (>500 h of continuous photoanodic water oxidation with < 10% decay in photocurrent

density). Figure S14 shows the *J-E* behavior of one electrode. Figure S15 show the comparison of the electrode surface morphology images before and after 40 hours operation in KOH. This observation combines with the discussion from Figure 4 indicated that the planar Si /NW GaAs/*a*-TiO_2/NiO_x electrode morphology did not experience significant change during the operation in 1M KOH in the early stage of first 40 hours either.

S3 Supplementary Figures and Tables

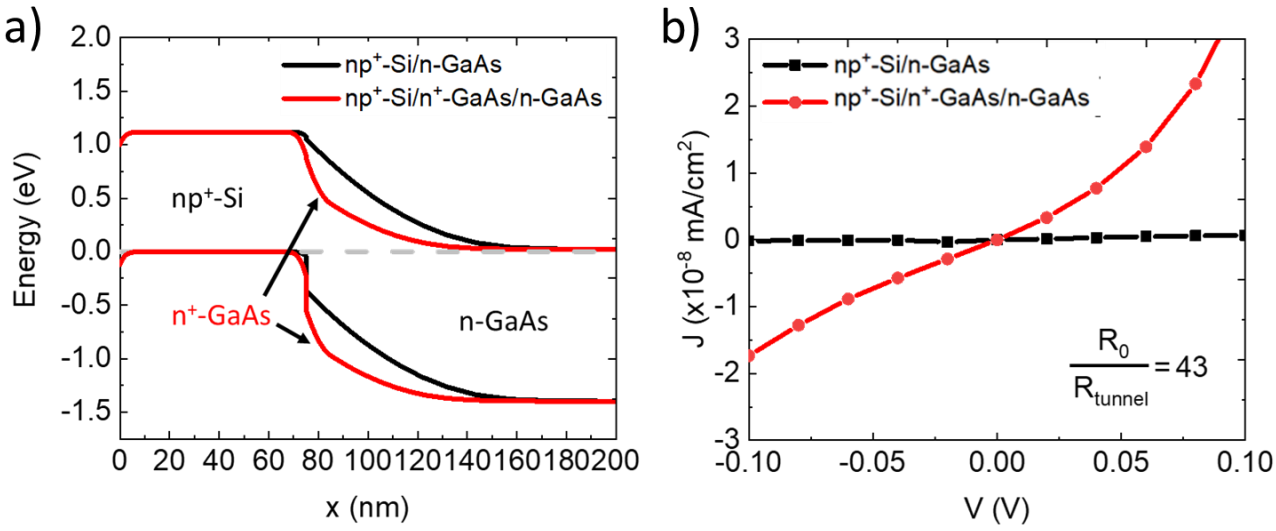

Figure S1. Simulation of (a) band diagram and (b) current density-voltage characteristics of the np$^+$-Si/n-GaAs junction without (black) and with (red) the n$^+$-GaAs seed layer (10 nm). R_0 and R_{tunnel} are the resistance of the p$^+$-Si/n-GaAs junctions without and with the n$^+$-GaAs seed layer, respectively.

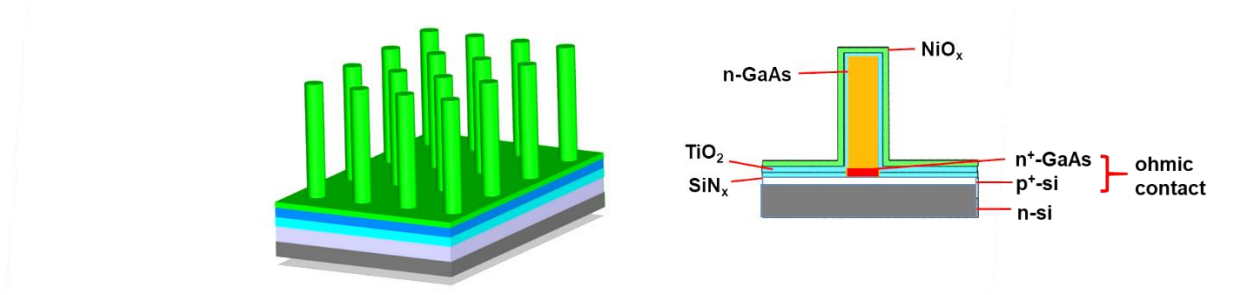

Figure S2. Schematics of the structure and layer components of the tandem planar Si /NW GaAs /*a*-TiO_2/NiO_x photoanode.

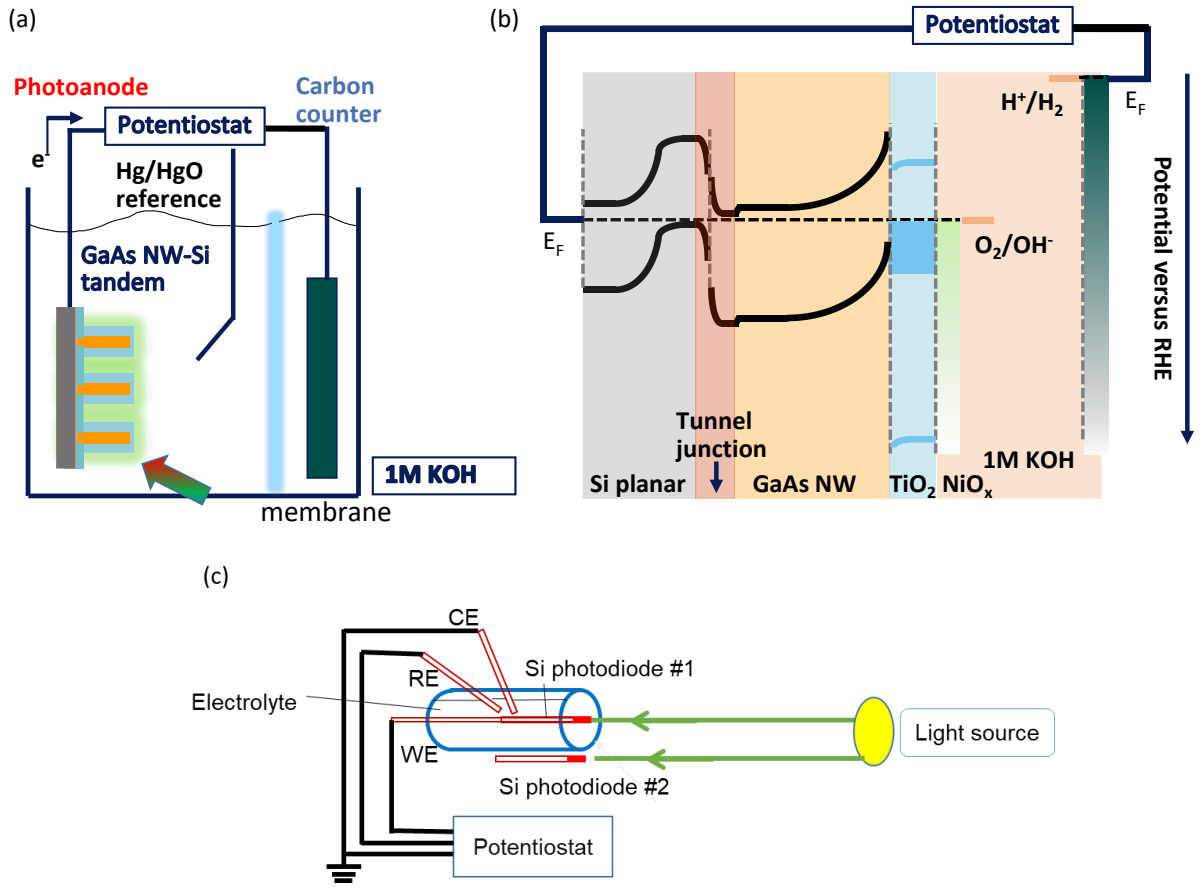

Figure S3. Schematic drawings of (a) the three-electrode cell for photoelectrochemical water oxidation; (b) the band structure of the tandem planar Si /NW GaAs /*a*-TiO_2/NiO_x photoanode, with an ohmic electrical contact between the top GaAs and bottom Si absorbers, drawn as a p^+-Si/n^+-GaAs ohmic junction; and (c) the placement of the photodiodes during light calibration process.

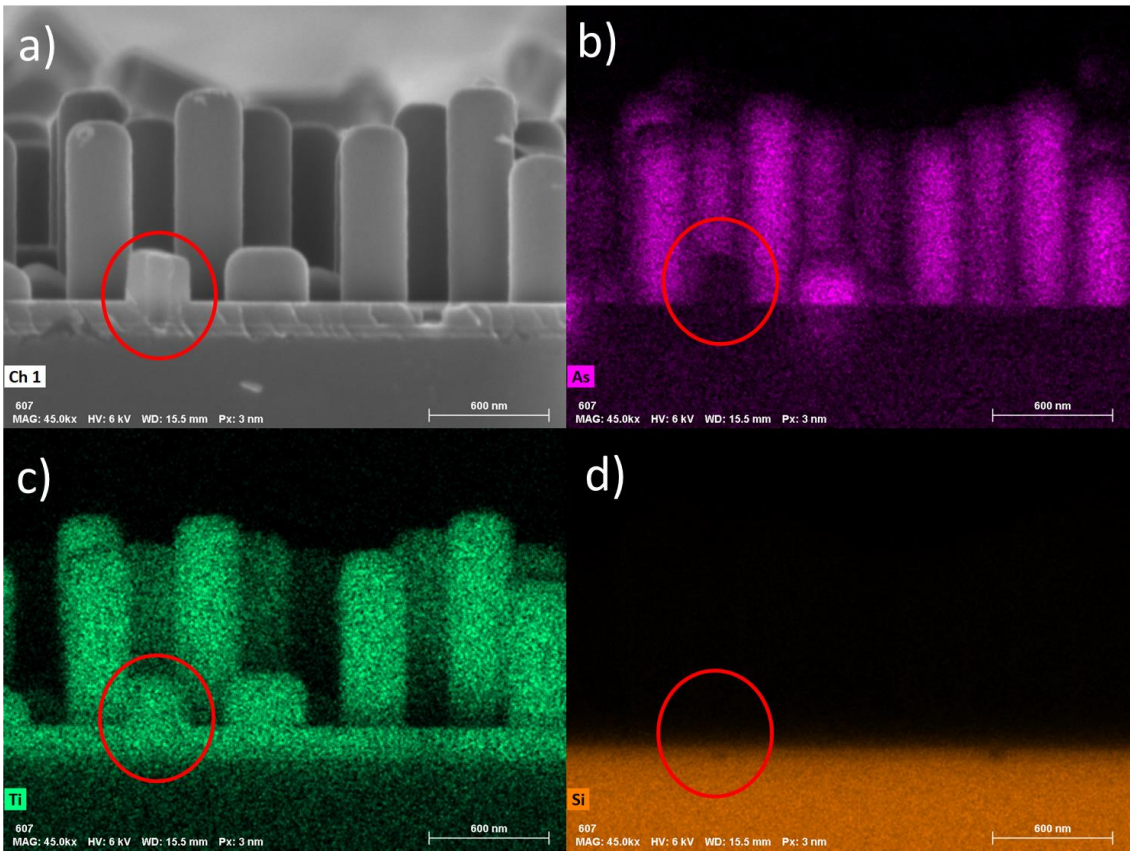

Figure S4. SEM of an empty TiO_2/NiO_x shell (marked by the red circle) on the planar Si/ GaAs NW/TiO_2/NiO_x electrode after 600 hours test. a) The cross-sectional image; (b)-(d) Elemental mapping for Ti, As, and Si of the region shown in a).

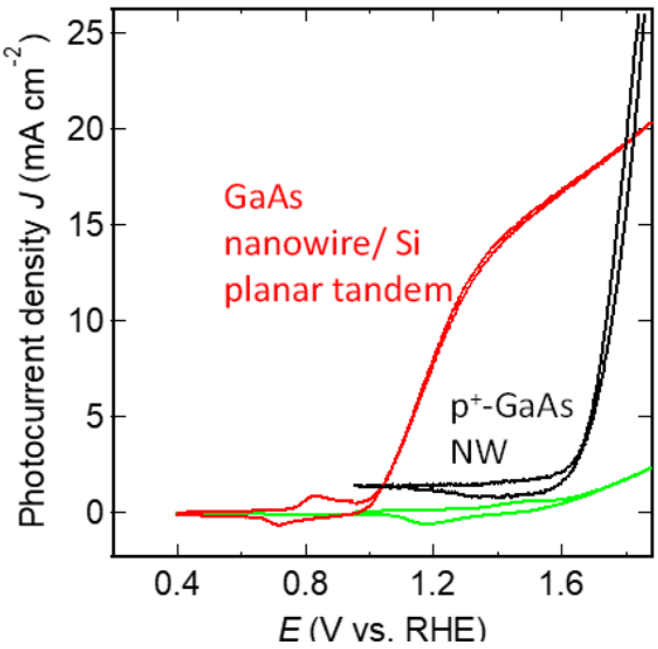

Figure S5. *J-E* behavior of planar Si /NW GaAs /*a*-TiO_2/NiO_x photoanodes under ~ 1.7 Sun intensity of illumination (red curve) and in the dark (green curve), respectively, overlaid with the dark *J-E* behavior of planar p^+-GaAs /NW p^+-GaAs /*a*-TiO_2/NiO_x anodes (black curve). The third cyclic voltammetric scan (black curve) of this p^+-GaAs nanowire anode showed evidence for corrosion, as indicated by the positive non-water-oxidation background current that increased continually as more scans were acquired. The scan rate is kept at 20 mV/s for all *J-E* measurements. The tests are conducted in 1M KOH.

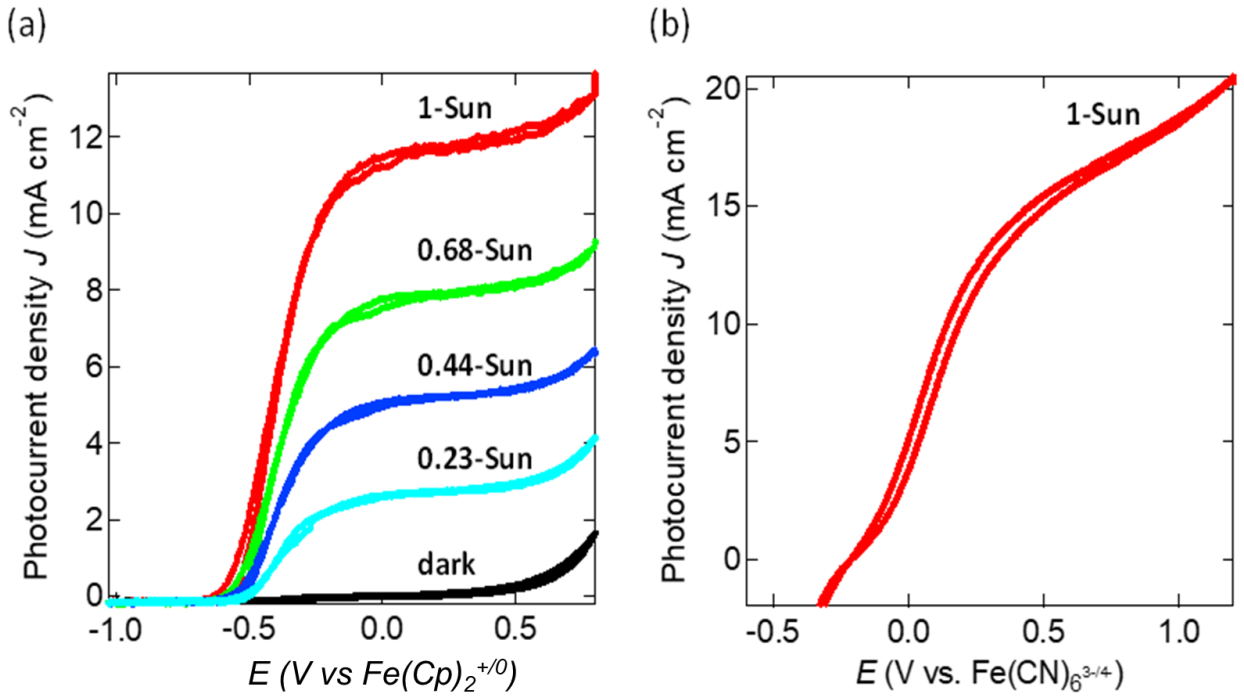

Figure S6. In contact with one-electron facile redox couples: (a) light-dependent *J-E* behavior of a top GaAs nanowire absorber (GaAs nanowire grown on GaAs planar substrate) measured in contact with 50 mM/90 mM $Fe(Cp)_2^{+/0}$ redox couples in a non-aqueous CH_3CN-$LiClO_4$ electrolyte; and (b) *J-E* behavior of a top GaAs nanowire absorber measured in contact with an aqueous 50 mM/350 mM $Fe(CN)_6^{3-/4-}$ electrolyte under simulated 1-sun illumination. The scan rate is kept at 20 mV/s for all *J-E* measurements.

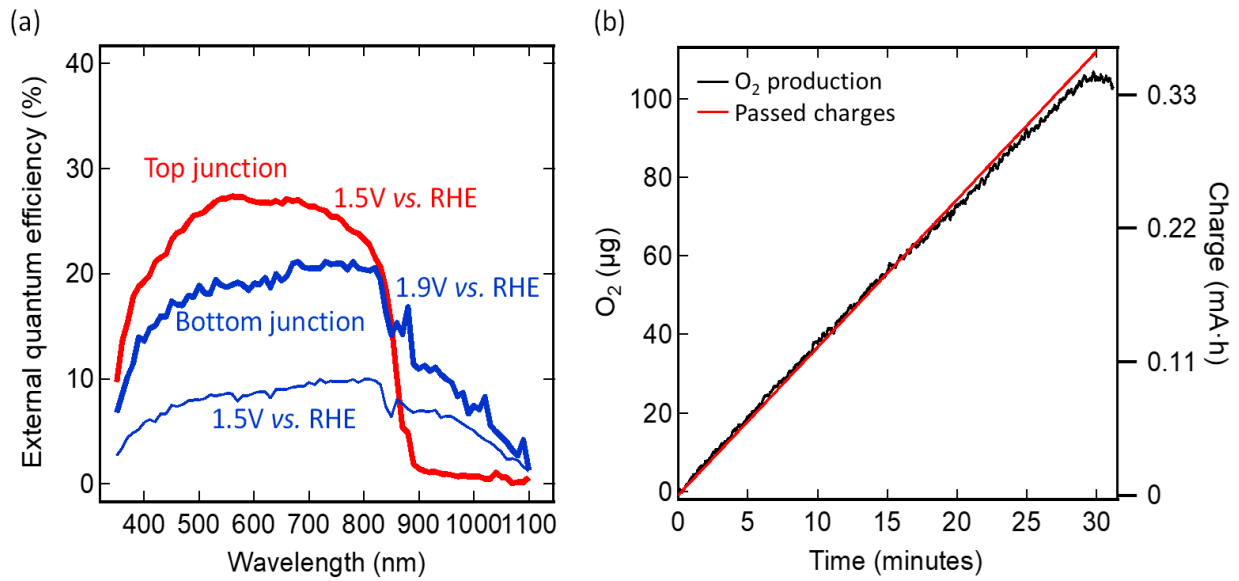

Figure S7. Quantitative analysis of tandem planar Si /NW GaAs /*a*-TiO_2/NiO_x photoanodes. (a) Spectral response of the top junction (red) and the bottom junction (blue), respectively, measured in contact with 1.0 M KOH(aq) at 1.5 V and 1.9 V vs RHE, respectively. (b) Overlay of the cumulative dissolved O_2(g) detected (dark) and of the charge passed (red) from 0 to 30 min of photoanode operation (test stopped at 30 min). The left axis and right axis ranges and ticks were scaled to match with each other, assuming 100% Faradaic efficiency for water oxidation to evolve O_2.

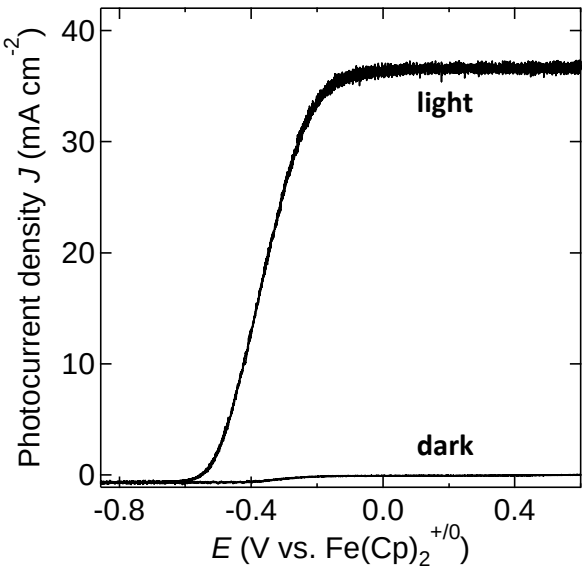

Figure S8. Energy-conversion performance of planar np^+-Si (111) buried junctions in contact with a non-aqueous $Fe(Cp)_2^{+/0}$ redox system. The two labeled curves indicate the *J-E* behavior measured under 1-sun illumination and in the dark, respectively. The scan rate is kept at 20 mV/s for all *J-E* measurements.

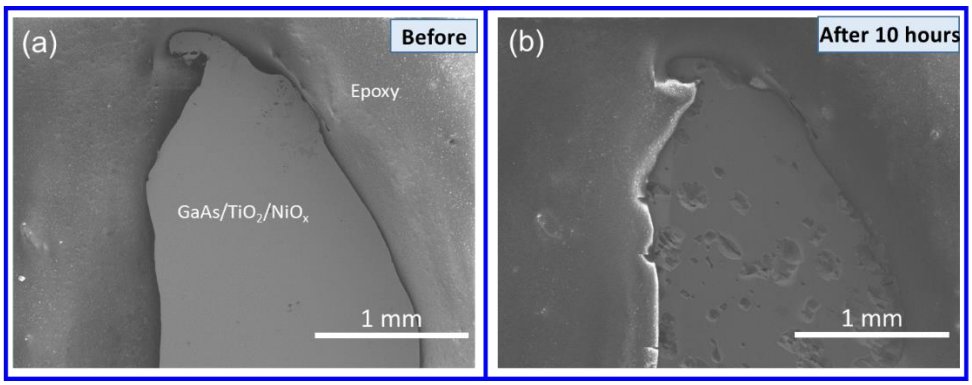

Figure S9. SEM micrographs of a planar n-GaAs/100 nm *a*-TiO_2/NiO_x photoelectrode surface. (a) Plan-view morphology of a planar GaAs/ *a*-TiO_2/NiO_x photoanode before stability testing; (b) plan-view morphology of a planar GaAs/*a*-TiO_2/NiO_x electrode after continuous operation in 1.0 M KOH (aq) for 10 h at 1.5 V vs. RHE under 1-sun illumination. Visible corrosion pits can be observed after testing.

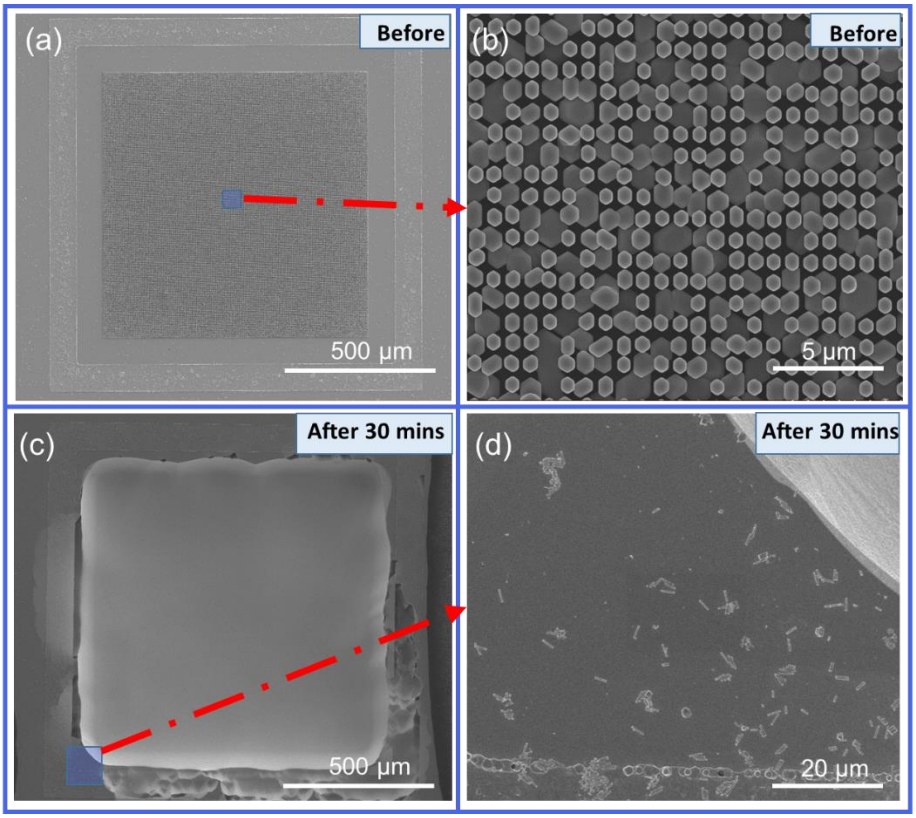

Figure S10. SEM micrographs of a planar GaAs /NW GaAs /100 nm *a*-TiO_2/NiO_x photoelectrode surface. (a) and (c) Plan-view morphology of a planar photoanode before and after, respectively, operation in 1.0 M KOH(aq) for 0.5 h at 1.5 V vs. RHE under 1-sun illumination, respectively. (b) and (d) are magnified micrographs of representative areas as marked by the small blue rectangular regions in (a) and (c), respectively.

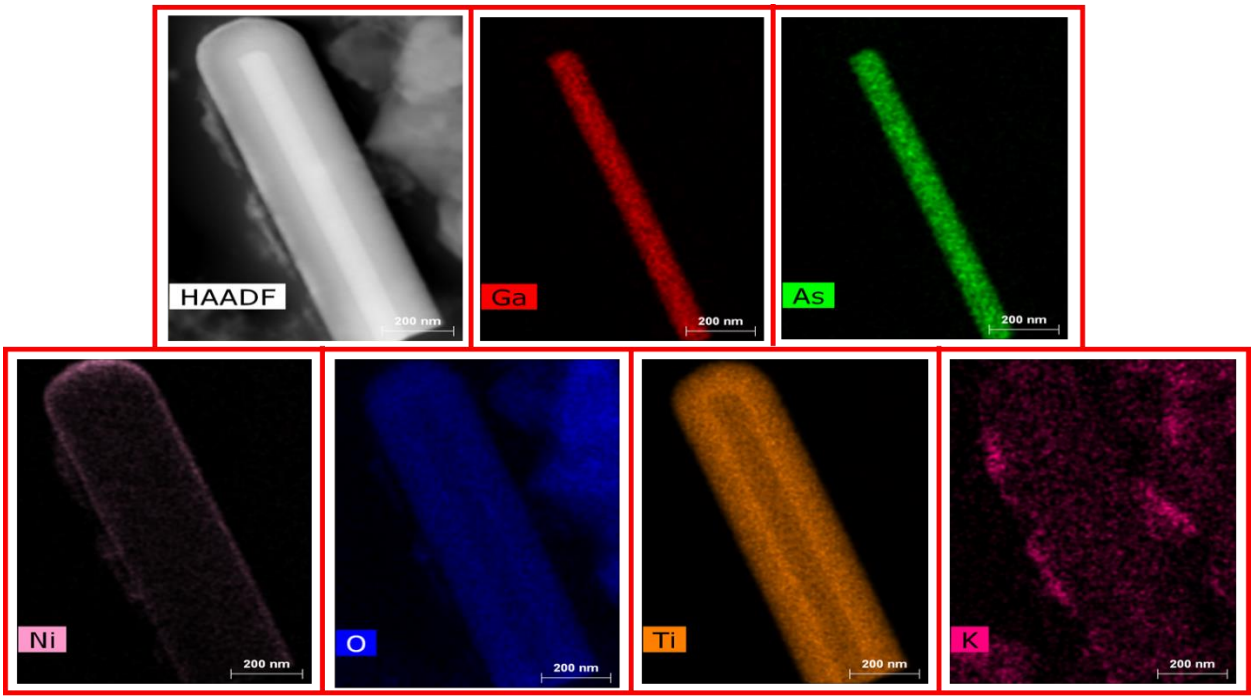

Figure S11. STEM-TEM micrographs and EDS mapping of an individual nanowire after 600 h of stability testing.

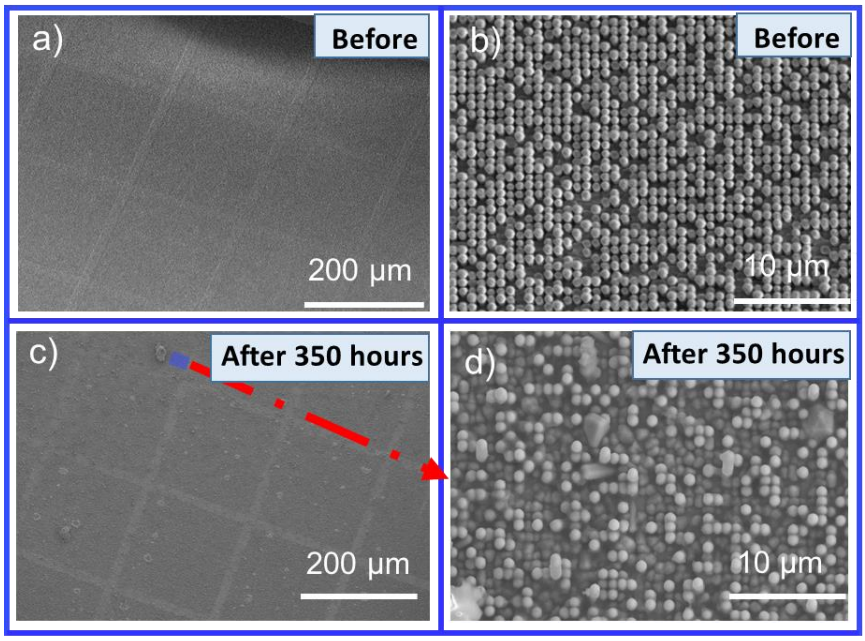

Figure S12. SEM micrographs of a tandem planar Si /NW GaAs /*a*-TiO_2/NiO_x photoelectrode (TiO_2 thickness of 20 nm) surface: plan-view images of the electrode (a) before the test, (c) after 350 h of operation in 1.0 M KOH(aq); and magnified images of the electrode (b) before the test, (d) after 350 h of operation in 1.0 M KOH(aq).

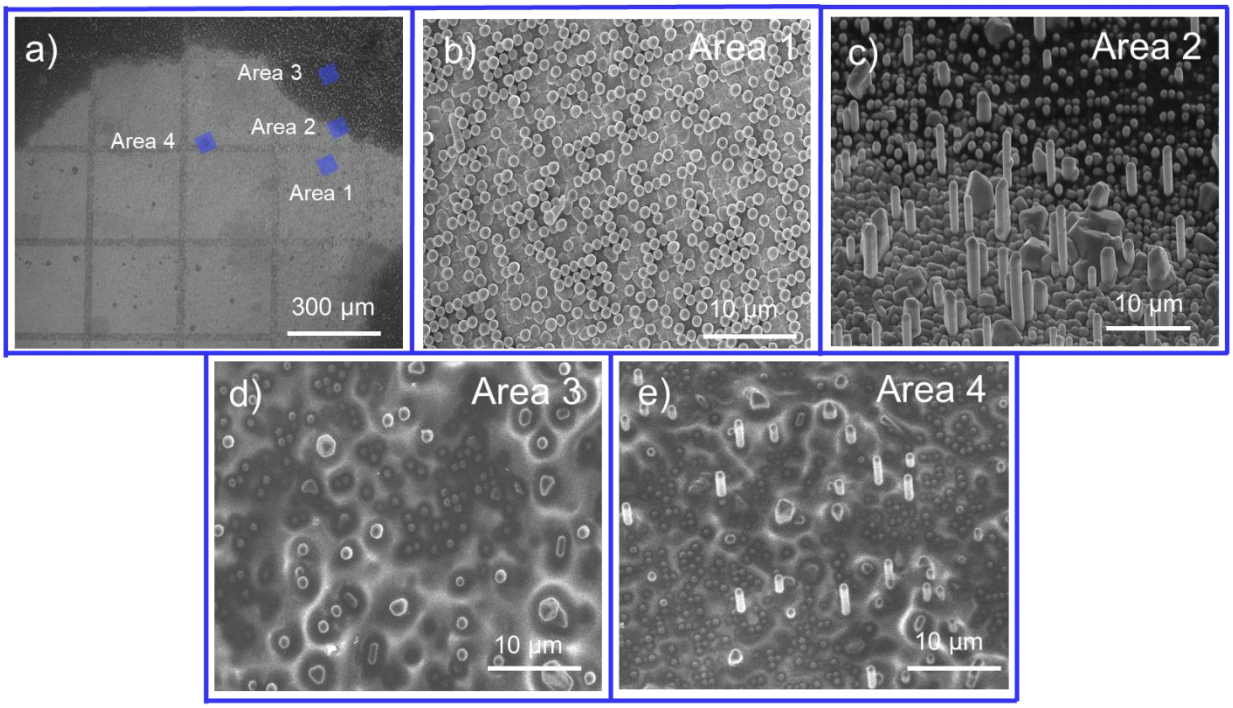

Figure S13. SEM micrographs of a tandem planar Si /NW GaAs /*a*-TiO_2/NiO_x photoanode (*a*-TiO_2 thickness of 5 nm) surface after 50 h of stability testing in 1.0 M KOH(aq): (a) plan-view image; (b) magnified image of the unaffected region; (c) magnified image at the boundary between the unaffected and corroded regions as the corrosion front propagates across the photoanode surface; (d) and (e) magnified images of the corroded region, either behind the corrosion front or surrounded by the unaffected region.

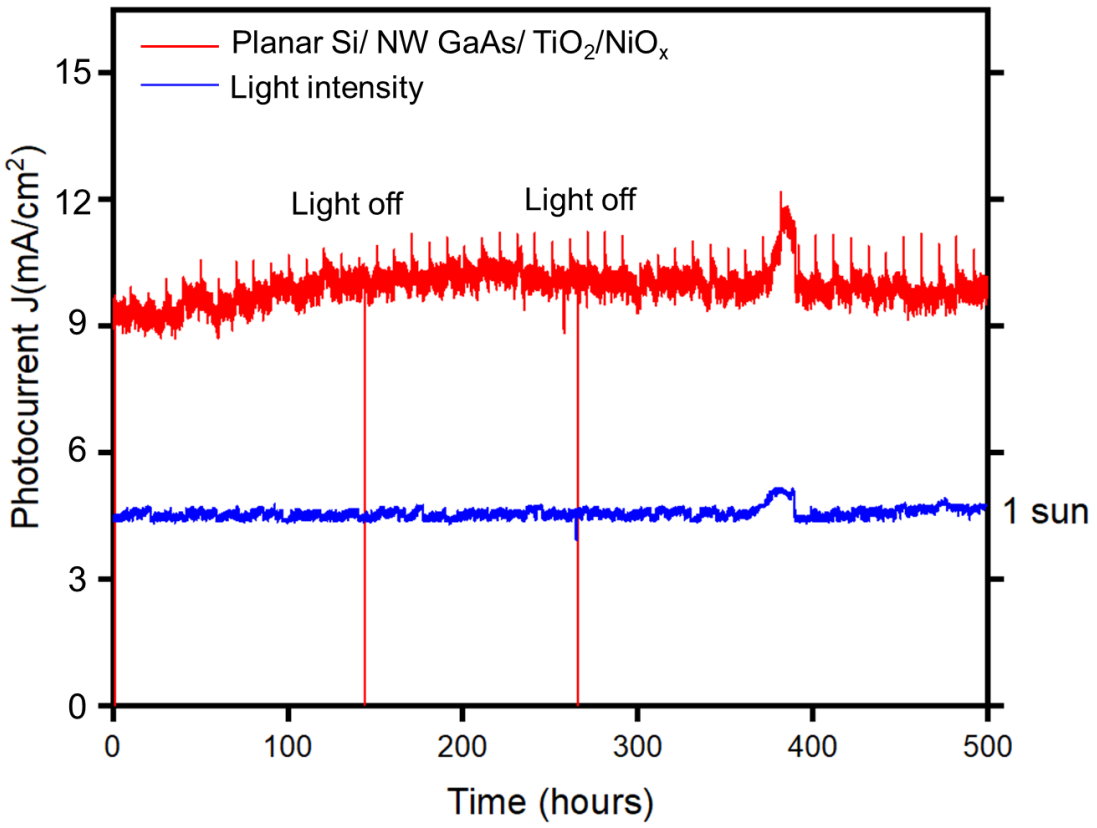

Figure S14. Another repeated experiment for 500 hours of continuous operation for tandem planar Si/NW GaAs/a-TiO_2/NiO_x photoanodes in 1M KOH: Time dependence of the anodic water oxidation current density (Red), held at 1.50 V vs. RHE (0.60 V vs. Hg/HgO), overlaid with the light intensity as a function of time (Blue).

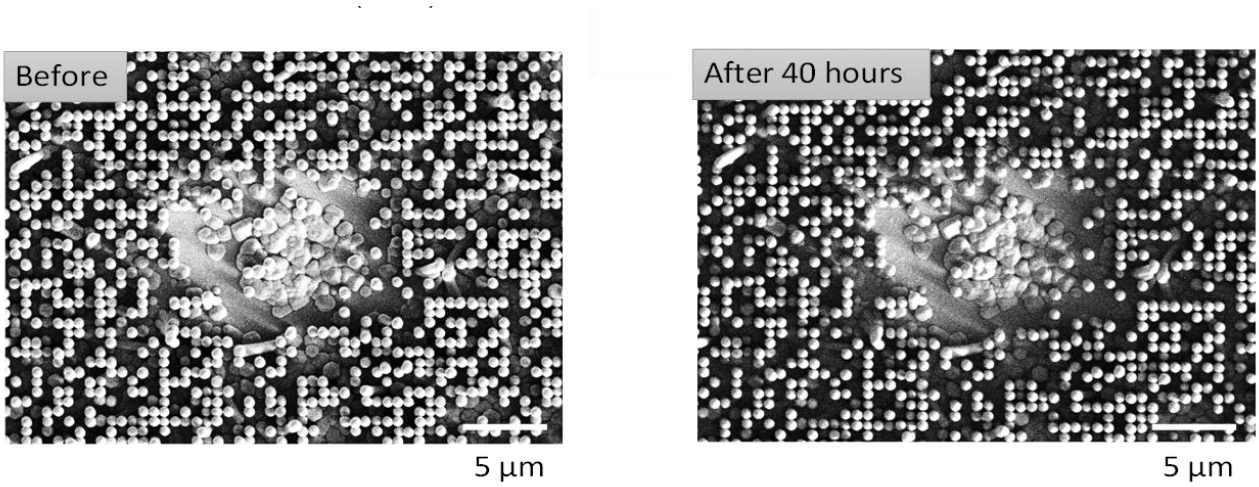

Figure S15. The SEM image of another Planar Si/ GaAs NW/TiO_2/NiO_x electrode before and after 40 hours operation in 1M KOH.

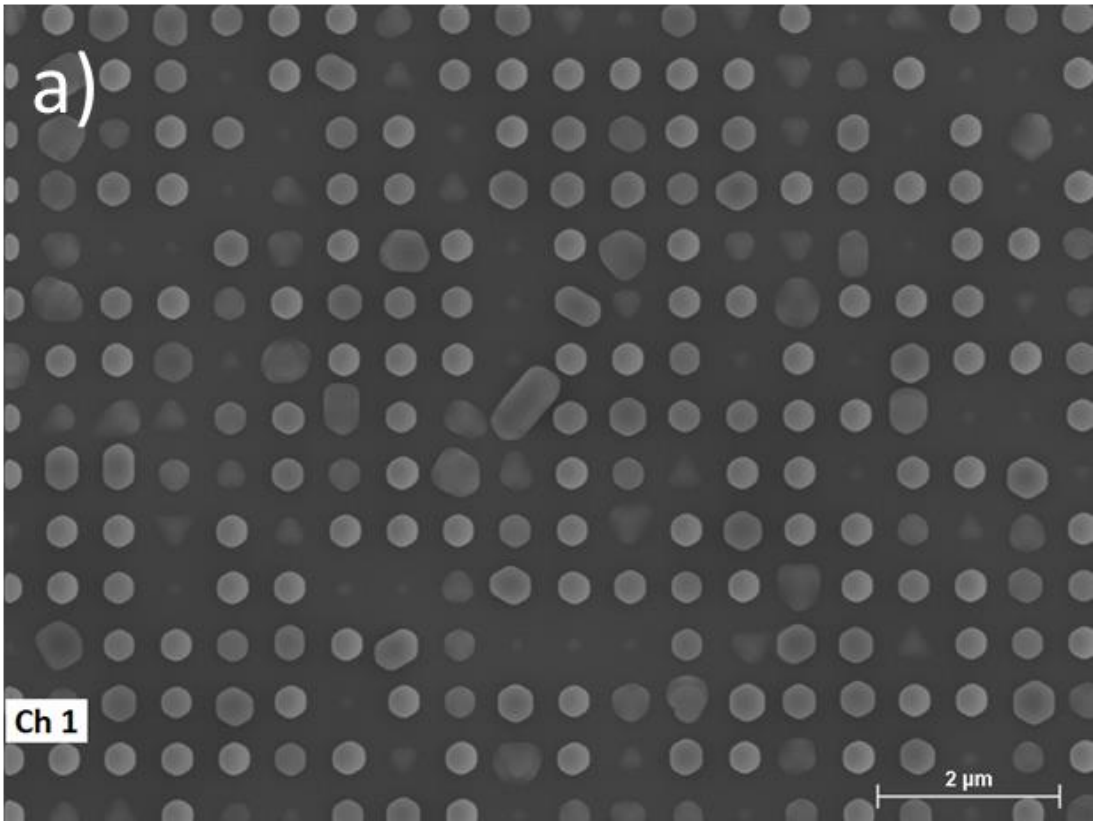
a)
Ch 1
2 µm

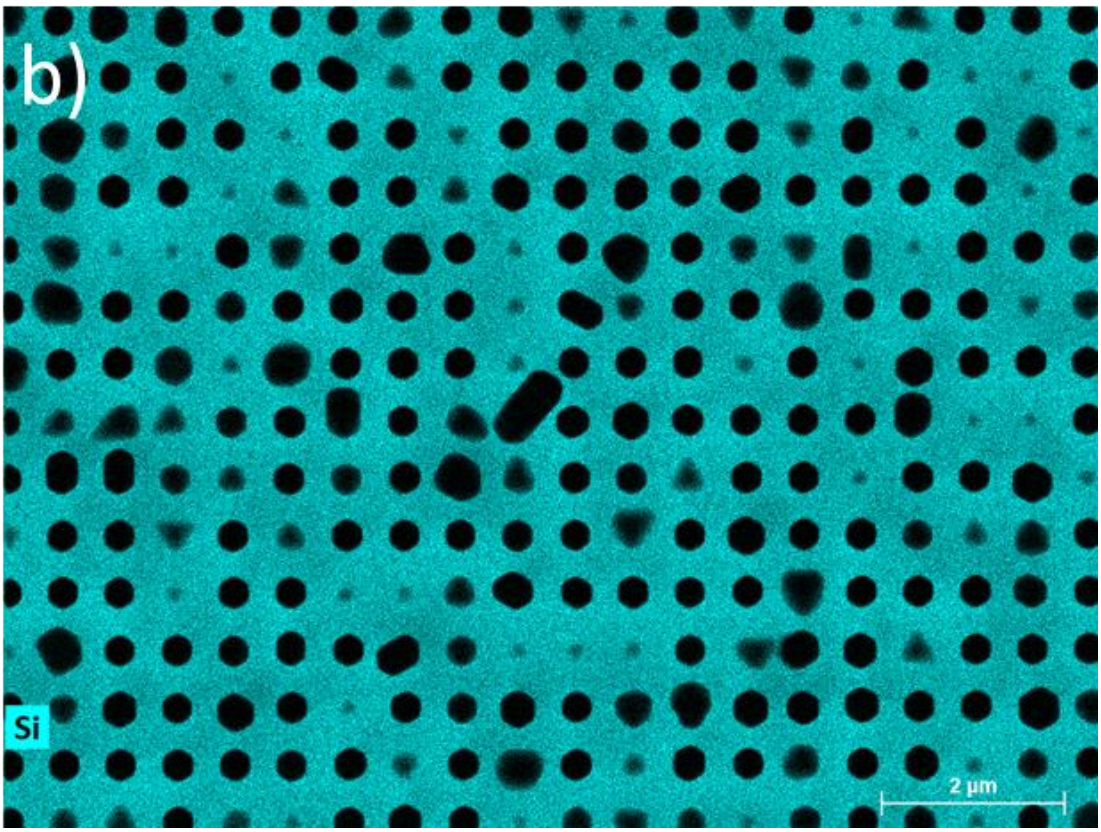
b)
Si
2 µm

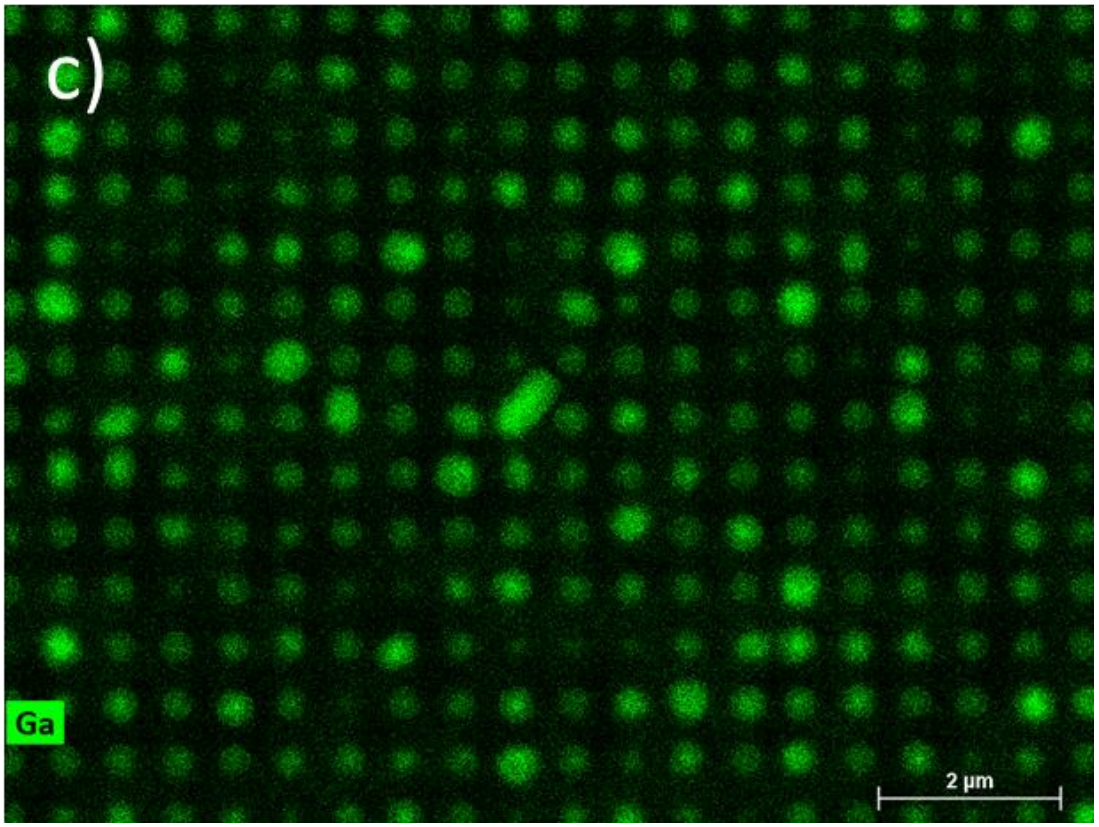
c)
Ga
2 µm

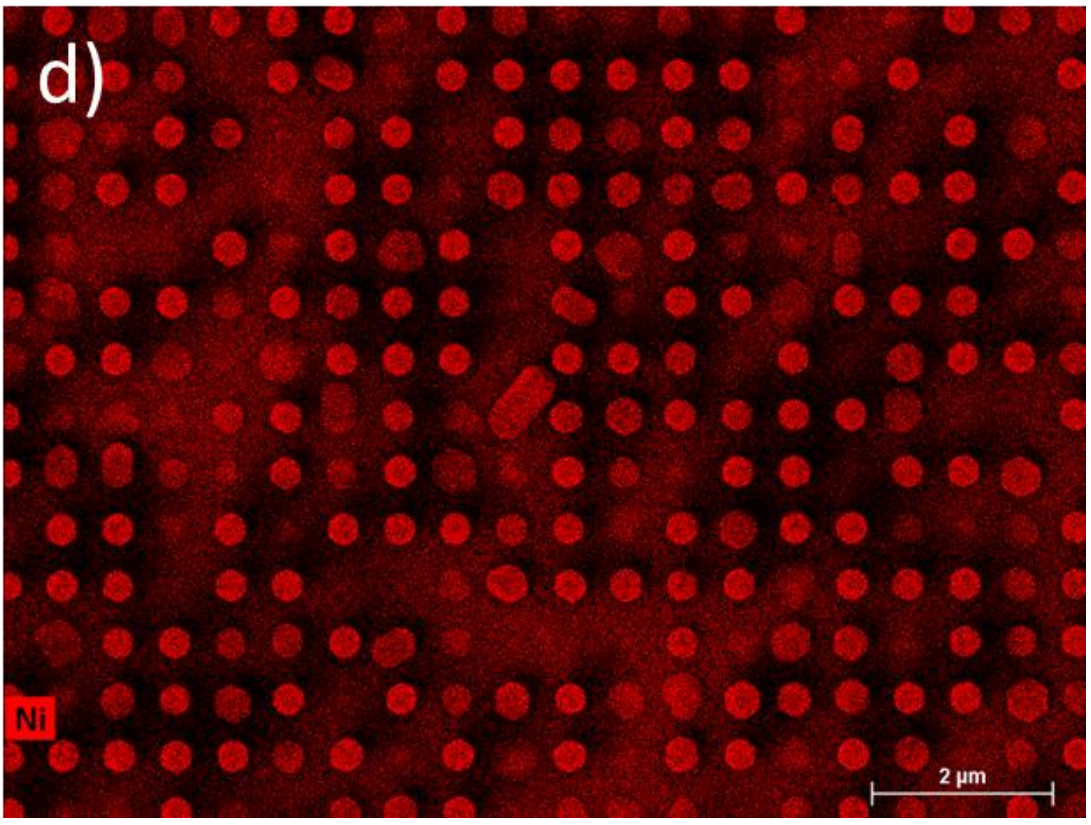
d)
Ni
2 µm

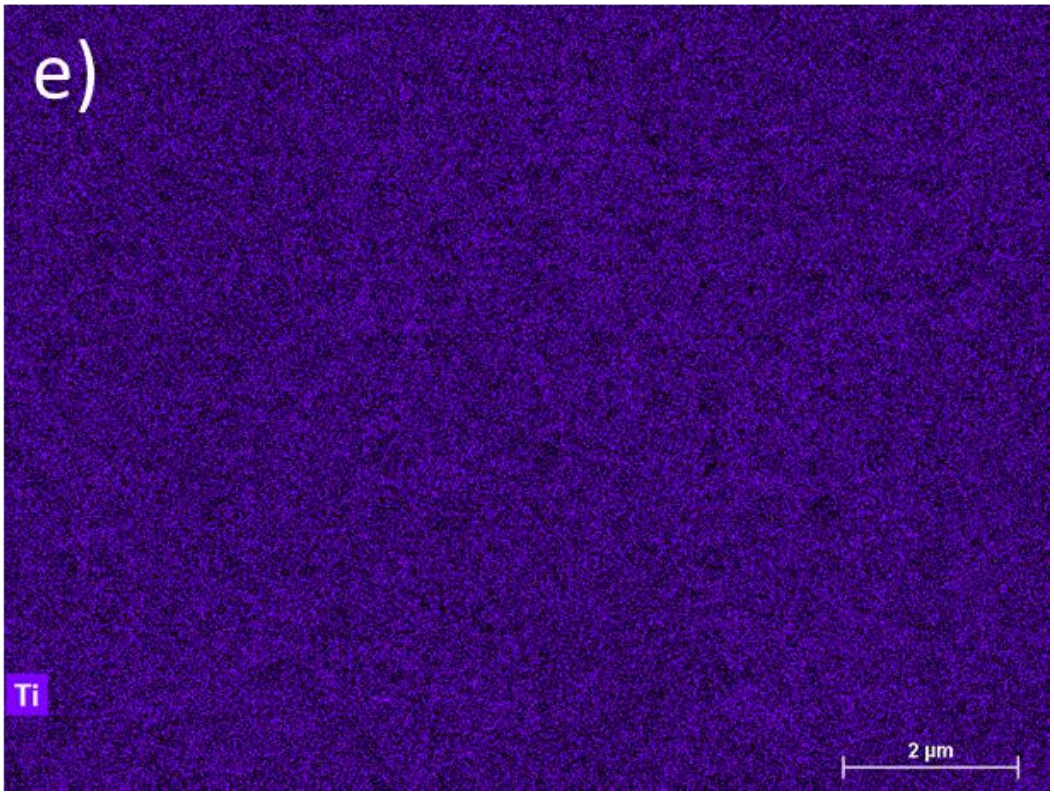
e)
Ti
2 µm

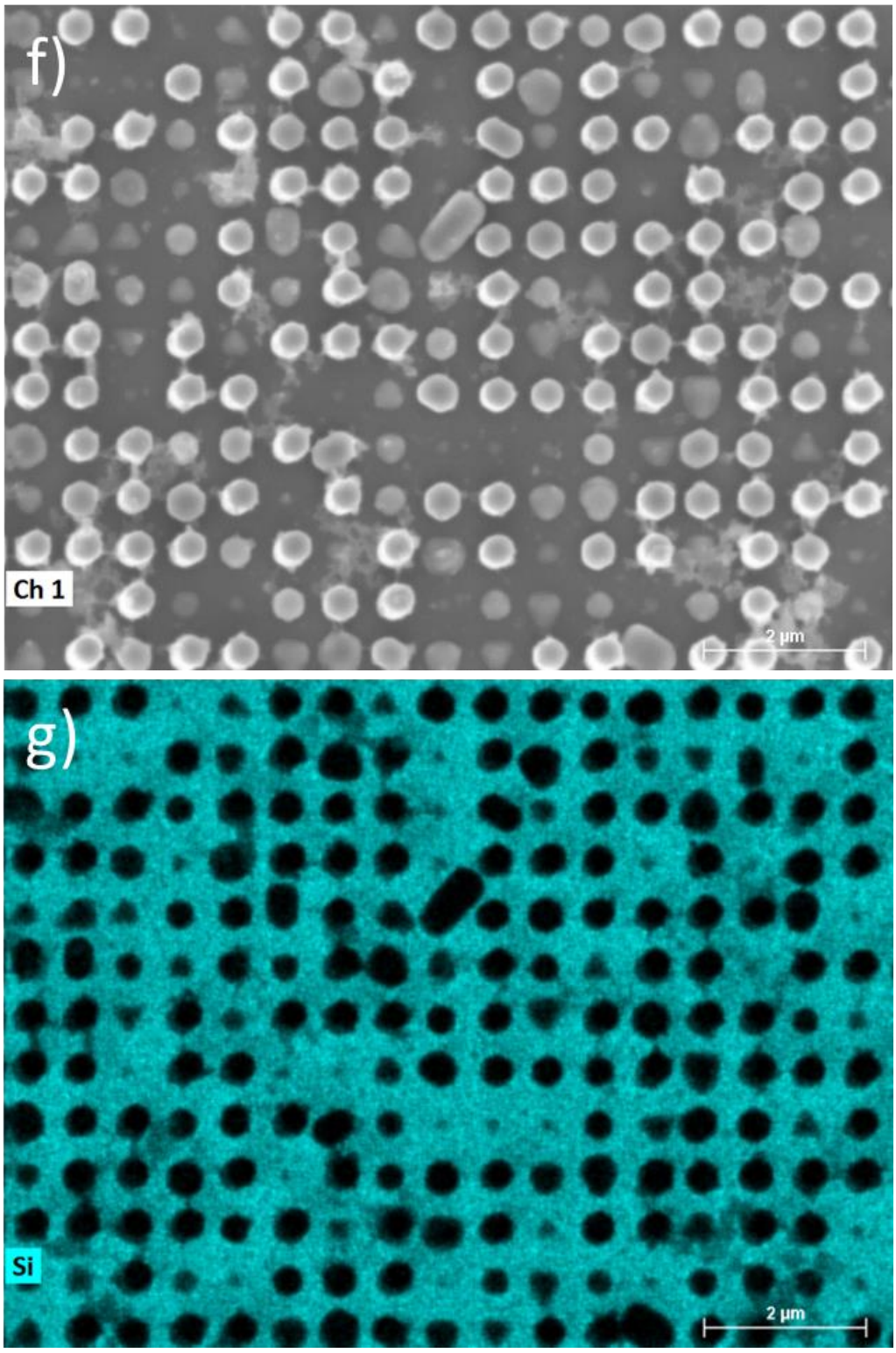
f)
Ch 1
2 µm
g)
Si
2 µm

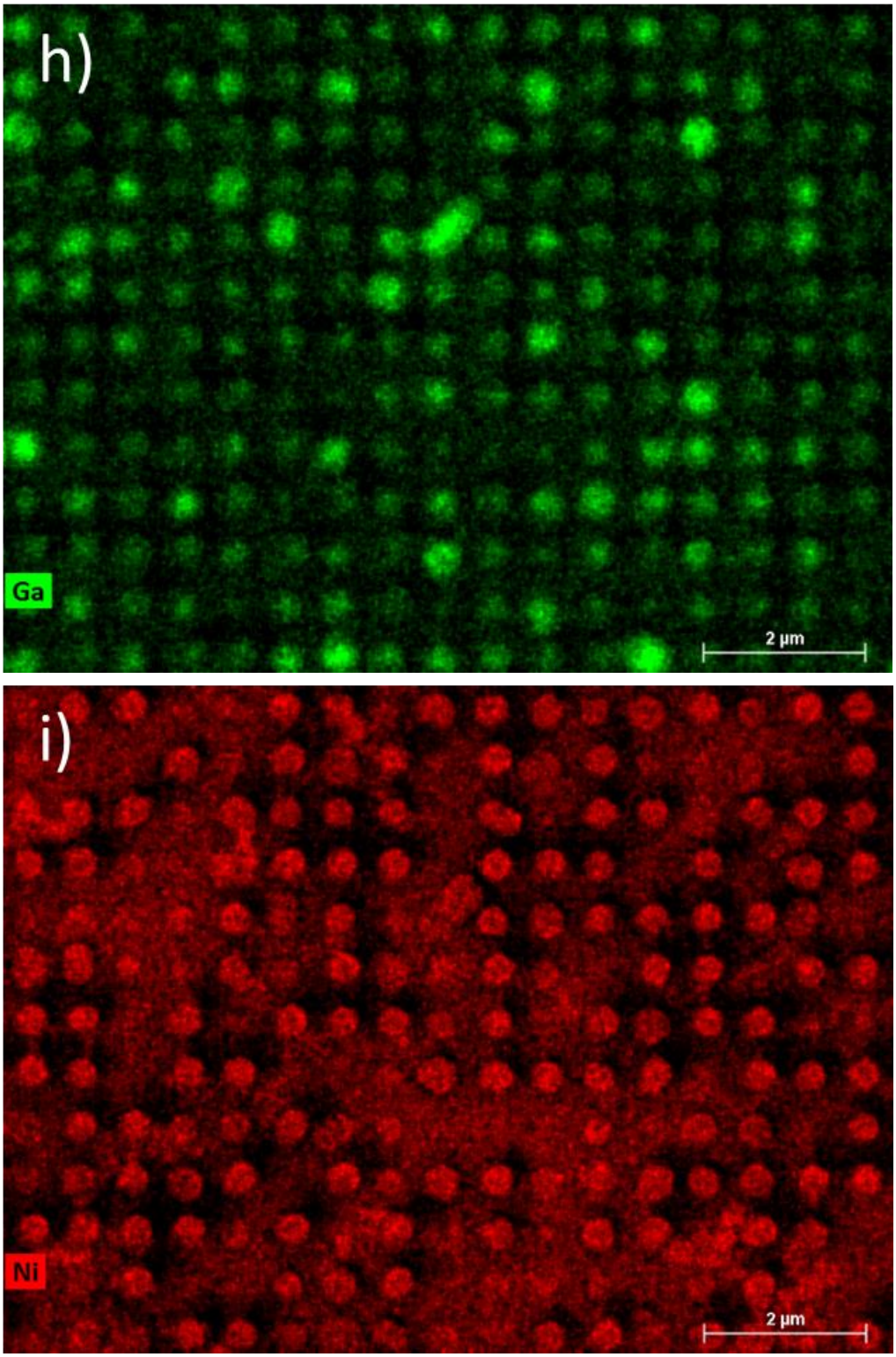
h)
Ga
2 µm
i)
Ni
2 µm

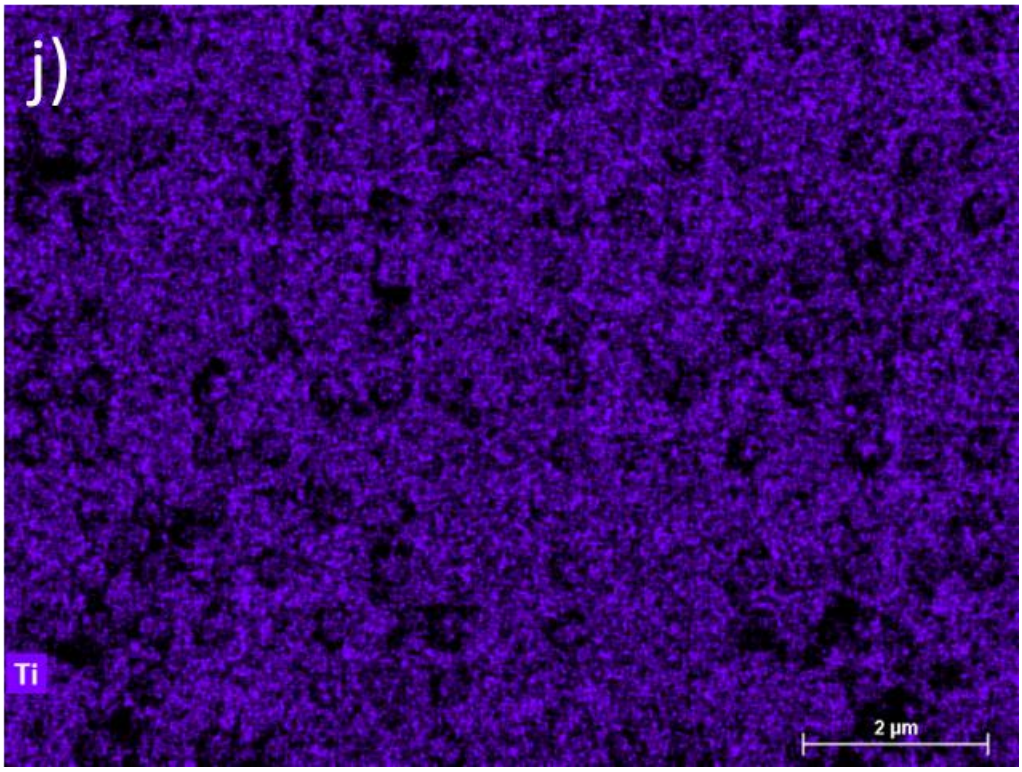

Figure S16. High-resolution reproduction for the SEM-EDS image of Figure 4. (a)-(e) Before the test; (f)-(j) After the 600 hours test.

Supplementary Table S1. Various photoelectrodes and the respective operational environments. (a) the photoelectrode structures; and (b) the respective three-electrode cell configuration implemented in the experimental and results sections.

(a)

Light absorber	Coating	Catalyst	Label	Purpose
Tandem planar np$^+$-Si(111) / nanowire n-GaAs	Amorphous TiO_2	NiO_x	Tandem planar Si /NW GaAs /*a*-TiO_2/NiO_x	Defect-mitigation design studied herein
planar p$^+$-GaAs / nanowire p$^+$-GaAs	Amorphous TiO_2	NiO_x	Tandem planar p$^+$-GaAs /NW p$^+$-GaAs /*a*-TiO_2/NiO_x	Evaluation of energy-conversion property and onset potentials
Planar np$^+$-Si(111)	/	/	Planar np$^+$-Si	Study of bottom photoabsorber properties in non-aqueous electrolytes
planar n$^+$-GaAs(111)B / nanowire n-GaAs	Amorphous TiO_2	NiO_x	planar GaAs /NW GaAs /*a*-TiO_2/ NiO_x	Study of TiO_2-coated top photoabsorber energy-conversion properties in aqueous electrolytes and comparison for defect tolerance study
planar n$^+$-GaAs(111)B / nanowire n-GaAs	/	/	planar GaAs /NW GaAs	Study of top photoabsorber properties in non-aqueous electrolytes
n-GaAs	Amorphous TiO_2	NiO_x	GaAs /*a*-TiO_2/ NiO_x	A comparison for defect tolerance study

(b)

Electrolyte	Ref	Counter	Purpose
1 M KOH (aq)	Hg/HgO	Carbon rod	Measurement of PEC water-oxidation performance and stability
$Fe(CN)_6^{3-/4-}$ (aq)	Pt wire	Pt gauze	Measurement of energy-conversion properties of n-GaAs with TiO_2 coatings and NiO_x catalysts
non-aqueous $Fe(Cp)_2^{+/0}$	Pt wire	Pt gauze	Measurement of energy-conversion properties of n-GaAs without the influence of corrosion
Different metallocene redox couples dissolved in 1.0 M $LiClO_4$ acetonitrile electrolytes	Pt wire	Pt gauze	Measurement of n-GaAs/redox liquid junction properties to show the influence of contacting layers

Supplementary Table S2. Nanowire density for the three randomly selected areas (marked by yellow dash squares, numbered as 1, 2, and 3) in **Figure 3b** (before stability test) and **Figure 3d** (after stability test), respectively.

Area	Number of nanowires
Figure (3b) 1	732
Figure (3d) 1	724
Intact wire ratio	0.989
Figure (3b) 2	327
Figure (3d) 2	311
Intact wire ratio	0.951
Figure (3b) 3	378
Figure (3d) 3	371
Intact wire ratio	0.981

Supplementary Table S3. Photovoltages of n-GaAs nanowire arrays (planar GaAs /NW GaAs electrodes) in contact with different redox couples dissolved in non-aqueous electrolytes. These redox couples span a 1.25-V difference in Nernstian solution potentials, and the photovoltages measured for the nanowire arrays varied over a range of 0.35 V. (V_{oc} refers to the difference between the E_{oc} under illumination and E_{oc} in the dark.)

Redox	Potential (V vs. $Cp_2Fe^{+/0}$)	V_{oc} (mV)	Std. Dev. of V_{oc} (mV)
$Cp_2Fe^{+/0}$	– 0.139	~ 600	20.4
$Me_{10}Cp_2Fe^{+/0}$	– 0.579	~ 400	17.2
$Cp_2Co^{+/0}$	– 1.391	~ 250	15.1

S4 References

(1) Hu, S.; Chi, C. Y.; Fountaine, K. T.; Yao, M. Q.; Atwater, H. A.; Dapkus, P. D.; Lewis, N. S.; Zhou, C. W., Optical, electrical, and solar energy-conversion properties of gallium arsenide nanowire-array photoanodes. *Energy Environ. Sci.* **2013,** *6*, 1879-1890.

(2) Huang, N. F.; Lin, C. X.; Povinelli, M. L., Limiting efficiencies of tandem solar cells consisting of III-V nanowire arrays on silicon. *J Appl Phys* **2012,** *112*, 064321.

(3) Yao, M. Q.; Cong, S.; Arab, S.; Huang, N. F.; Povinelli, M. L.; Cronin, S. B.; Dapkus, P. D.; Zhou, C. W., Tandem Solar Cells Using GaAs Nanowires on Si: Design, Fabrication, and Observation of Voltage Addition. *Nano Lett.* **2015,** *15*, 7217-7224.

(4) Bessire, C. D.; Bjork, M. T.; Schmid, H.; Schenk, A.; Reuter, K. B.; Riel, H., Trap-Assisted Tunneling in Si-InAs Nanowire Heterojunction Tunnel Diodes. *Nano Lett.* **2011,** *11*, 4195-4199.

(5) Yang, T.; Hertenberger, S.; Morkotter, S.; Abstreiter, G.; Koblmuller, G., Size, composition, and doping effects on In(Ga)As nanowire/Si tunnel diodes probed by conductive atomic force microscopy. *Appl. Phys. Lett.* **2012,** *101*, 233102.

(6) Hu, S.; Shaner, M. R.; Beardslee, J. A.; Lichterman, M.; Brunschwig, B. S.; Lewis, N. S., Amorphous TiO_2 coatings stabilize Si, GaAs, and GaP photoanodes for efficient water oxidation. *Science* **2014,** *344*, 1005-1009.

(7) Shaner, M. R.; Hu, S.; Sun, K.; Lewis, N. S., Stabilization of Si microwire arrays for solar-driven H_2O oxidation to O_2(g) in 1.0 M KOH(aq) using conformal coatings of amorphous TiO_2. *Energy Environ. Sci.* **2015,** *8*, 203-207.

(8) Huang, N. F.; Lin, C. X.; Povinelli, M. L., Broadband absorption of semiconductor nanowire arrays for photovoltaic applications. *J Optics* **2012,** *14*, 024004.

(9) Yu, Y. H.; Sun, C. L.; Yin, X.; Li, J.; Cao, S. Y.; Zhang, C. Y.; Voyles, P. M.; Wang, X. D., Metastable Intermediates in Amorphous Titanium Oxide: A Hidden Role Leading to Ultra-Stable Photoanode Protection. *Nano Lett.* **2018,** *18*, 5335-5342.

(10) Buabthong, P.; Ifkovits, Z. P.; Kempler, P. A.; Chen, Y. K.; Nunez, P. D.; Brunschwig, B. S.; Papadantonakis, K. M.; Lewis, N. S., Failure modes of protection layers produced

by atomic layer deposition of amorphous TiO_2 on GaAs anodes. *Energy Environ. Sci.* **2020,** *13*, 4269-4279.

(11) Ros, C.; Carretero, N. M.; David, J.; Arbiol, J.; Andreu, T.; Morante, J. R., Insight into the Degradation Mechanisms of Atomic Layer Deposited TiO_2 as Photoanode Protective Layer. *ACS Applied Materials & Interfaces* **2019,** *11*, 29725-29735.